SPECTROSCOPIC CONFIRMATION OF AN ULTRA-MASSIVE GALAXY IN A PROTOCLUSTER AT $z\sim 4.9$[*]

Stephanie M. Urbano Stawinski[1,†], M. C. Cooper[1], Ben Forrest[2], Adam Muzzin[3], Danilo Marchesini[4], Gillian Wilson[5], Percy Gomez[6], Ian McConachie[7], Z. Cemile Marsan[3], Marianna Annunziatella[8], and Wenjun Chang[7]

[1]Department of Physics & Astronomy, University of California, Irvine, 4129 Reines Hall, Irvine, CA 92697, USA
[2]Department of Physics and Astronomy, University of California Davis, One Shields Avenue, Davis, CA 95616 USA
[3]Department of Physics and Astronomy, York University, 4700, Keele Street, Toronto, ON MJ3 1P3, Canada
[4]Department of Physics and Astronomy, Tufts University, 574 Boston Avenue, Medford, MA 02155, USA
[5]Department of Physics, University of California Merced, 5200 North Lake Rd., Merced, CA 95343, USA
[6]W.M. Keck Observatory, 65-1120 Mamalahoa Hwy., Kamuela, HI 96743, USA
[7]Department of Physics & Astronomy, University of California Riverside, 900 University Ave., Riverside, CA 92521 USA and
[8]Centro de Astrobiología (CSIC-INTA), Ctra de Torrejón a Ajalvir, km 4, E-28850 Torrejón de Ardoz, Madrid, Spain
Version April 25, 2024

ABSTRACT

We present spectroscopic confirmation of an ultra-massive galaxy (UMG) with $\log(M_\star/M_\odot) = 10.98 \pm 0.09$ at $z_{\rm spec} = 4.8947$ in the Extended Groth Strip (EGS), based on deep observations of Lyα emission with Keck/DEIMOS. The ultra-massive galaxy (UMG-28740) is the most massive member in one of the most significant overdensities in the EGS, with four additional photometric members with $\log(M_\star/M_\odot) > 10.5$ within $R_{\rm proj} \sim 1$ cMpc. Spectral energy distribution (SED) fitting using a large suite of star formation histories and two sets of high-quality photometry from ground- and space-based facilities consistently estimates the mass of this object to be $\log(M_\star/M_\odot) \sim 11$ with a small standard deviation between measurements ($\sigma = 0.09$). While the best-fit SED models agree on stellar mass, we find discrepancies in the estimated star formation rate for UMG-28740, resulting in either a star-forming or quiescent system. *JWST*/NIRCam photometry of UMG-28740 strongly favors a quiescent scenario, demonstrating the need for high-quality mid-IR observations. Assuming the galaxy to be quiescent, UMG-28740 formed the bulk of its stars at $z > 10$ and is quenching at $z \sim 8$, resulting in a high star formation efficiency at high redshift ($\epsilon \sim 0.2$ at $z \sim 5$ and $\epsilon \gtrsim 1$ at $z \gtrsim 8$). As the most massive galaxy in its protocluster environment, UMG-28740 is a unique example of the impossibly early galaxy problem.

Subject headings: galaxies:high-redshift – galaxies:evolution – galaxies:clusters

1. INTRODUCTION

The discovery of extremely massive, passive galaxies at $z \sim 3-4$ has challenged our understanding of galaxy formation and evolution at early times (Glazebrook et al. 2017; Schreiber et al. 2018; Forrest et al. 2020a,b; Valentino et al. 2020). These quiescent ultra-massive galaxies (UMGs, $M_\star > 10^{11}$ M$_\odot$) have little to no ongoing star formation, requiring a period of intense, bursty star formation followed by rapid quenching within the first 2 Gyr of the Universe. Such extreme systems are difficult to reproduce in galaxy formation models, with current simulations struggling to form UMGs so early in cosmic time and and often failing to quench these systems by $z \sim 3$ (Forrest et al. 2020a; Valentino et al. 2023; Xie et al. 2024). Thus, although rare, confirmation of UMGs provide powerful constraints on theoretical models of galaxy formation and evolution (e.g. Baugh 2006; Croton et al. 2006; Nelson et al. 2018).

Intriguingly, the modeled ages and star formation histories of UMGs at $z \sim 3$ suggest that some systems assembled the majority of their mass and subsequently quenched as early as $z \sim 5$ (Forrest et al. 2020b; Schreiber et al. 2018). Overall, there appears to be rapid evolution of the UMG population at $4 < z < 6$, as some of these massive systems transition from highly star-forming to passive. Imaging campaigns that

originally uncovered UMGs at $z \sim 3$ also corroborate these findings, yielding samples of photometric UMG candidates at $z > 4$ (e.g. Muzzin et al. 2013a,b; Weaver et al. 2023). Meanwhile, measurements of the number density of UMGs find a significant increase in their abundance with cosmic time from $z \sim 6$ to $z \sim 3$ (Stefanon et al. 2015; Davidzon et al. 2017; Marsan et al. 2022; Weibel et al. 2024). Altogether, deep photometric surveys point to not only the existence of these extreme systems at $z \sim 5$, but also that this epoch is critical for understanding the rapid evolution of this extreme population.

While it is presumed that ultra-massive galaxies should exist at $z \sim 5$, spectroscopic confirmation of candidate systems has been challenging. Studies searching for UMGs at $z \sim 5$ have encountered difficulty in identifying and detecting these systems via both ground- and space-based spectroscopy (Antwi-Danso et al. 2023; Marsan et al. in prep). The few existing, spectroscopically-confirmed UMGs at $z > 4$ represent a biased population of systems with exceptionally high star formation rates (SFR $\gtrsim 500$ M$_\odot$ yr^{-1}) and with relatively poorly-constrained stellar masses (e.g. Xiao et al. 2023, but see also Carnall et al. 2023).

Herein, we present the discovery of a spectroscopically-confirmed, ultra-massive ($M_\star \sim 10^{11}$ M$_\odot$) galaxy at $z = 4.8947$ that resides within an extreme overdense region in the Extended Groth Strip (EGS). In §2, we describe our target selection criterion and spectroscopic observations. We present the resulting spectral fitting and characterization of the protocluster environment in §3. We discuss the competing star formation histories (SFH), compare our object to existing

simulations, and investigate the mass assembly history of this object in §4. Finally, we summarize our results in §5. Unless otherwise specified, we adopt a ΛCDM cosmology throughout with $\Omega_M = 0.3$, $\Omega_\Lambda = 0.70$, and $H_0 = 68$ km s^{-1} Mpc^{-1} (Planck Collaboration et al. 2016).

2. DATA

2.1. *Target Selection and Photometric Measurements*

We selected UMG candidates ($M_\star \gtrsim 10^{11}$ M$_\odot$) at $3.5 < z_{phot} < 6.5$ in the Extended Groth Strip (EGS) using the multi-wavelength photometric catalog from the Cosmic Assembly Near-infrared Deep Extragalactic Legacy Survey (CANDELS; Grogin et al. 2011; Koekemoer et al. 2011). The CAN-DELS photometric catalog (Stefanon et al. 2017), which spans $0.4 - 8\mu m$ via a suite of ground- and space-based imaging, incorporates photometric redshifts and stellar masses from seven separate photo-z codes and/or spectral energy distribution (SED) template sets. For selection purposes, we used the median z_{phot} and $M_\star$ reported in the catalog. To increase the likelihood of detection of Lyα, we prioritized objects that had an apparent CFHT r-band AB magnitude of < 28 and star formation rate (SFR) of $\gtrsim 100$ M$_\odot$ yr^{-1}. To increase our sample size, we included UMG candidates within the given redshift range that had lower SFRs and masses as filler targets.

UMG-28740 ($\alpha = 14^h19^m39.7^s$ and $\delta = +52°56^m56.5^s$), in particular, was selected as a star-forming candidate, with an estimated SFR of $20 - 200$ M$_\odot$ yr^{-1} and an apparent CFHT r-band magnitude of $27.9^{+0.6}_{-0.4}$. Within the Stefanon et al. (2017) catalog, UMG-28740 has a median photometric redshift of $z_{phot} = 4.495$ and a median stellar mass of $\log(M_\star/M_\odot) = 11.0$. In total, the CANDELS catalog reports photometric measurements of UMG-28740 at $ugriz$ and JHK_s bands from CFHT, F606W, F814W, F125W, F140W, and F160W from *HST*, as well as all four *Spitzer*/IRAC channels.

In addition to the photometry from CANDELS, this galaxy was recently observed with *JWST*/NIRCam (Rieke et al. 2003; Beichman et al. 2012) as part of the Cosmic Evolution Early Release Survey (CEERS, PID 12117; Finkelstein et al. 2023; Bagley et al. 2023). Using *JWST*/NIRCam (pointing 2), UMG-28740 was observed with the F115W, F150W, F200W, F277W, F356W, F410M, and F444W filters at a 5σ depth ranging from AB magnitudes of $28.35-29.2$. While the CEERS photometry was not incorporated in the initial target selection, it is utilized in this work as a supplemental set of photometry in §3.1.

2.2. *Spectroscopic Observations and Reduction*

Using Keck/DEIMOS (Faber et al. 2003), we observed UMG-28740 in March and May of 2023 on three different slitmasks. For all observations, we used the 600 lines mm^{-1} grating blazed at 7500 Å and tilted to a central wavelength of 7200 Å, with the GG455 order-blocking filter employed and no dithering between exposures. With slit widths of $1''$, the spectral resolution (FWHM) for the 600g grating on DEIMOS is ~ 3.5 Å (Weiner et al. 2006), with a dispersion of 0.65 Å per pixel. Calibrations for each slitmask included three internal quartz lamp flat-field frames and an arc lamp spectrum (using Kr, Ar, Ne, and Xe lamps). We were able to observe UMG-28740 with the three different slitmasks for a combined exposure time of 6.9 hours. The average seeing for these observations ranged from ~ 0.8-$1''$ with variable transparency.
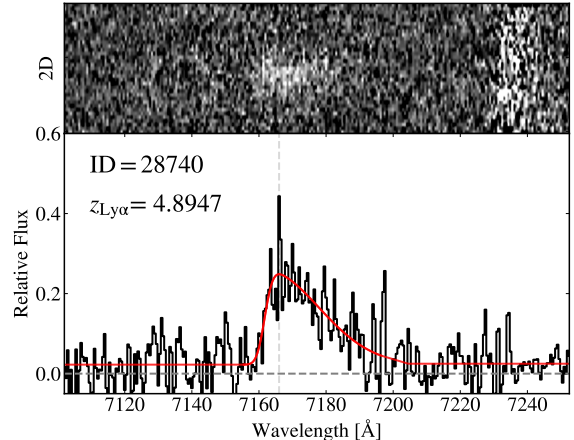
The Keck/DEIMOS observations were reduced using the

FIG. 1.— (*top*) A ~ 150 Å-wide section of the co-added 2D spectrum for UMG-28740 from our Keck/DEIMOS observations, highlighting the Lyman-α emission line. (*bottom*) The corresponding co-added 1D spectrum with the resulting best-fit redshift shown in red.

spec2d[1] DEEP2/DEEP3 DEIMOS data reduction pipeline (Newman et al. 2013; Cooper et al. 2012), yielding sky-subtracted, wavelength-calibrated 1D and 2D spectra for each target. We then combined the three 1D spectra of UMG-28740 from the reduction of each slitmask, creating a final co-added 1D spectrum as shown in Figure 1. For visualization of the line, we also co-added the corresponding 2D spectra, as shown in the top panel of Figure 1.

To measure a best-fit redshift, we utilized a custom template fitter (as used in Urbano Stawinski et al. 2024) that incorporates both an emission-line galaxy template as well as an asymmetric Gaussian profile to probe for a single Lyα line. For UMG-28740, we found a single emission line nearby the expected wavelength for Lyα given the photometric redshift. Fitting this profile, we find the resulting heliocentric-corrected spectroscopic redshift for UMG-28740 is $z_{spec} = 4.8947$ (best-fit model is shown by the red line in Fig. 1).

While this redshift is determined by the presence of a single emission line, there are multiple arguments consolidating this feature to be Lyα. First, the asymmetric profile of the emission line follows the characteristic shape of Lyα emitters at $z > 3$ (e.g. Verhamme et al. 2008; Martin et al. 2015). Second, the measured redshift is consistent with two sets of photometry from CANDELS and CEERS, including high-quality photometric measurements from *HST*/WFC3 and *JWST*/NIRCam (see Fig. 2). Lastly, the location of this galaxy coincides with a large overdense region at $z \sim 5$ (first highlighted by Naidu et al. 2022 and later discussed in §3.2), which further solidifies $z_{spec} = 4.8947$ as the correct redshift.

3. ANALYSIS

3.1. *SED Fitting*

With our measured spectroscopic redshift ($z_{spec} = 4.8947$), we re-fit the SED of UMG-28740. Here, we employ both the photometry from CANDELS (Stefanon et al. 2017) and from CEERS (Bagley et al. 2023). From the CANDELS photometric catalog, we exclude the *HST*/ACS photometry at $F606W$ and $F814W$ due to uncertainties related to sky subtraction, such that the SED fits are made to the photome-
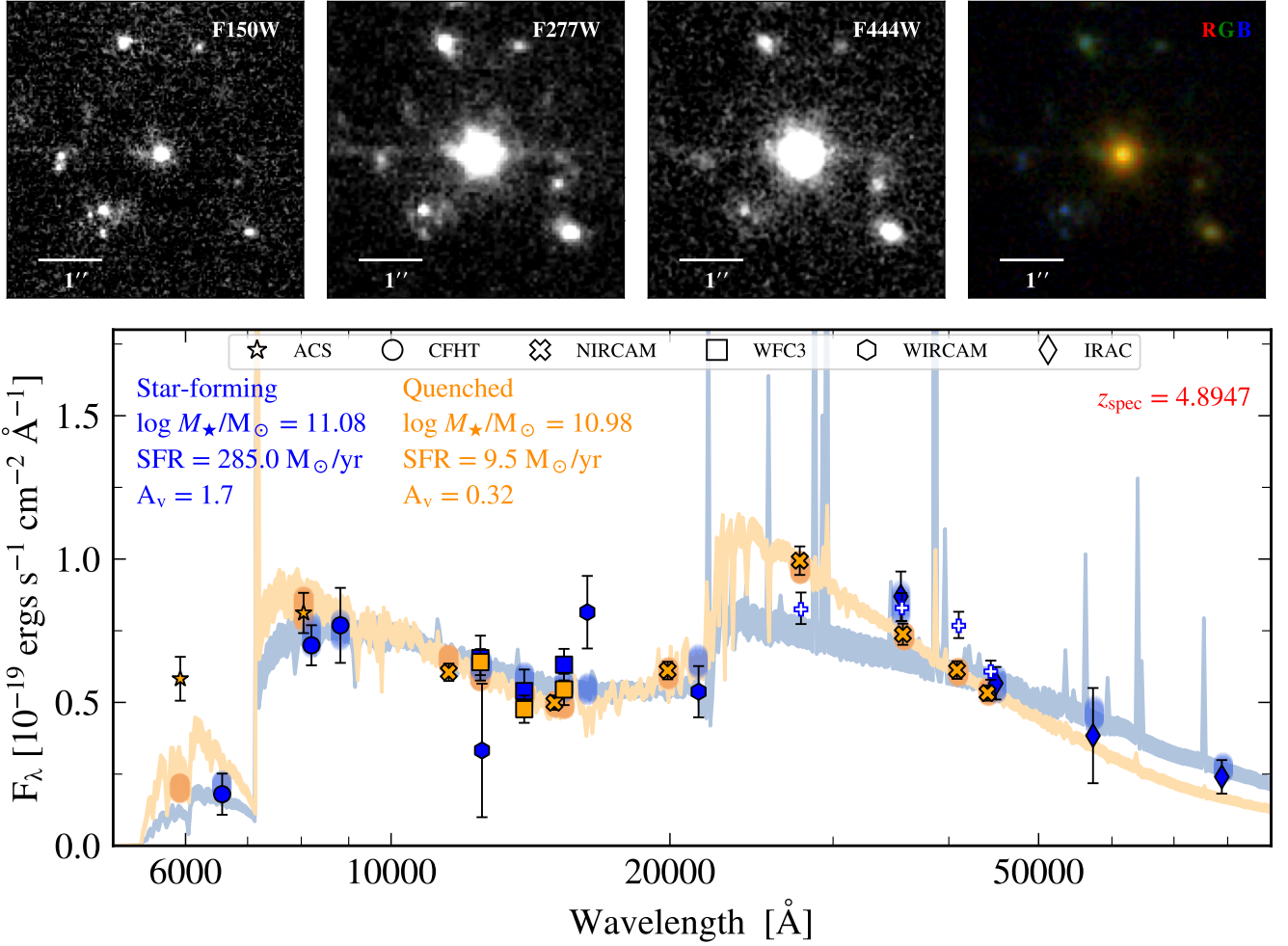
[1] https://sites.uci.edu/spec2d/

FIG. 2.— (*top*) From left to right: image stamps of UMG-28740 in the *JWST*/NIRCam 1.50μm, 2.77μm, and 4.44μm filters, followed by an RGB image (F150M in blue, F277M in green, and F444W in red). (*bottom*) Best-fit SEDs (star-forming in blue and quenched in orange) from BAGPIPES forced at the measured $z_{\rm spec}$. The two sets of observed photometry are shown as dark blue (Stefanon et al. 2017) and orange (Bagley et al. 2023) markers. The width of each SED indicates the $\pm 1\sigma$ confidence intervals resulting from BAGPIPES. The open blue crosses show the predicted *JWST*/NIRCam flux at F277W, F356W, F410M, and F444W for the blue star-forming SED. Here, the predicted *JWST*/NIRCam flux for the star-forming scenario is under-estimated at 2.77μm and over-estimated at $3.56 - 4.44$μm, suggesting that UMG-28740 is likely quenched.

try at $ugrizJHK_s$ from CFHT, F125W, F140W, and F160W from *HST*/WFC3-IR, and all four *Spitzer*/IRAC channels. Meanwhile, the CEERS catalog includes photometric measurements at F606W and F814W from *HST*/ACS, F125W, F140W, and F160W from *HST*/WFC3-IR, and finally F115W, F150W, F200W, F277W, F356W, F410M, and F444W from *JWST*/NIRCam.

The majority of our SED analysis was completed using the SED-fitting code Bayesian Analysis of Galaxies for Physical Inference and Parameter EStimation or BAGPIPES[2] (Carnall et al. 2018). BAGPIPES assumes Bruzal and Charlot stellar populations (Bruzual & Charlot 2003), a Kroupa IMF (Kroupa & Boily 2002), and a Calzetti dust law (Calzetti et al. 2000). Adopting a double-power law star formation history, we measure best-fit model SEDs for each set of photometry (from CANDELS and CEERS). The SEDs are fit to 10 free parameters, allowing for variation in metallicity, age, the slope of the Calzetti dust law, and the ionization parameter. The full set of free parameters used and their allowed distributions are outlined in Table 1.

[2] https://github.com/ACCarnall/bagpipes

As shown in Figure 2, the resulting SED fits give a stellar mass of $\log(M_\star/M_\odot) = 10.98^{+0.04}_{-0.03}$ using the CEERS photometry and $\log(M_\star/M_\odot) = 11.08^{+0.08}_{-0.1}$ using the CANDELS photometry. While the stellar mass is tightly constrained between the two sets of photometry, we find that the SFR is dependant on the photometric catalog utilized. The CANDELS photometry yields a dusty, highly star-forming galaxy (SFR $= 285.0^{+125.5}_{-79.5}$ $M_\odot$ yr^{-1}) and the fit to the *JWST*/NIRCam photometry produces a very low star formation rate (SFR $= 9.5^{+4.8}_{-2.7}$ $M_\odot$ yr^{-1}) and low dust attenuation. The latter, *nearly* quenched SED is shown in orange in Figure 2, and is consistent with both sets of photometry within $\pm 1\sigma$ error. On the other hand, the star-forming SED (shown in blue in Fig. 2) has insufficient emission in the rest-frame optical (~ 4000-6000Å), so as to under-produce the flux measured in the *JWST*/NIRCam F277W band. In addition, the star-forming SED overpredicts the observed flux in the *JWST*/NIRCam F356W, F410M, and F444W bands due to contribution from strong emission lines such as Hα at ~ 3.9μm. Based on the photometry alone, this favors the quenched scenario for UMG-28740 (see §4.1 for a more detailed discussion of these

TABLE 1
LIST OF FREE PARAMETERS USED IN THE SED FITS WITH BAGPIPES

Parameter	Unit	Range	Prior
General[a]			
Stellar Mass Formed	$M_\star/M_\odot$	(1, 15)	Logarithmic
Peak Star Formation	τ/Gyr	(0.3, t_{obs})	Logarithmic
Age	t_{age}/Gyr	(0.1, 1)	Logarithmic
Metallicity	$Z/Z_\odot$	(0.01, 2.5)	Logarithmic
V-band attenuation	A_V	(0, 8)	Uniform
Deviation from Calzetti slope	δ	(-0.3, 0.3)	Gaussian[b]
2175Å bump strength	B	(0, 5)	Uniform
Ionization	U	(-4, -2)	Logarithmic
Double-power law[c]			
double-power law falling slope	α	(0.01, 1000)	Logarithmic
double-power law rising slope	β	(0.01, 1000)	Logarithmic
Burst[d]			
Stellar Mass Formed	$M_\star/M_\odot$	(0, 15)	Logarithmic
Age	t_{age}/Gyr	(0.1, 1)	Logarithmic
Metallicity	$Z/Z_\odot$	(0.01, 2.5)	Logarithmic
AGN[d]			
Continuum Flux at 5100Å	f_{5100} erg/s/cm^2/Å	(0, 10^{-19})	Uniform
Hα Flux	$f_{H\alpha}$ erg/s/cm^2	(0, $10^{-16.6}$)	Uniform
Hα Velocity Dispersion	$\sigma_{H\alpha}$/km/s	(1000, 5000)	Logarithmic
Power law slope: at $\lambda < 5000$Å	$\alpha_{\lambda<5000}$	(-2, 2)	Gaussian[e]
at $\lambda > 5000$Å	$\alpha_{\lambda>5000}$	(-2, 2)	Gaussian[f]

[a]Parameters used in all SED fits.

[b]The Gaussian distribution for the Calzetti slope has a mean of $\mu = 0$ and a standard deviation of $\sigma = 0.1$

[c]Parameters specifically used in the double-power law fits.

[d]Parameters used in added AGN and burst components.

[e]The Gaussian distribution for the power law slope at $\lambda < 5000$Å has a mean of $\mu = -1.5$ and a standard deviation of $\sigma = 0.5$

[f]The Gaussian distribution for the power law slope at $\lambda > 5000$Å has a mean of $\mu = 0.5$ and a standard deviation of $\sigma = 0.5$

discrepancies).

To test the robustness of our measurements for mass and SFR, we ran BAGPIPES again using a variety of different models; varying the included free parameters, changing the assumed star formation history, restricting the assumed metallicity to solar, and adding different components such as bursts and an active galactic nucleus (AGN). In summary, we highlight the results from five different models: a double-power law SFH, a double-power law SFH including an AGN, a burst, or fixing the metallicity to solar metallicity, and a delayed-τ model (see Table 2). Adding an AGN or burst component is of interest to the evolution of massive galaxies in the early Universe, as the spectra of a subset of UMGs have significant AGN contributions (Marsan et al. 2017; Forrest et al. 2020b, Forrest et al. in prep.) and current theoretical models speculate that the rapid formation of such systems require extreme bursts of star formation (Sun et al. 2023).

We also compared the results from BAGPIPES to fits using the C++-adapted SED fitting code FAST++[3] (Kriek et al. 2009). With FAST++, we adopt the same parameters used in the

literature to model UMGs at $z \sim 3.5$ (Forrest et al. 2020a,b), assuming a Bruzal Charlot stellar population (Bruzual & Charlot 2003), the Calzetti dust law (Calzetti et al. 2000), and a Chabrier IMF (Chabrier 2003). The Chabrier IMF is related to the Kroupa IMF used in BAGPIPES by a factor of ~ 1 (Wright et al. 2017), allowing for direct comparison between results of the two SED codes. We allow FAST++ to vary the extinction from $0 < A_V < 4$ with a $\Delta A_V = 0.1$, the age from $7 < \log(\text{Age}) < $ age of the Universe at z_{spec} with $\Delta \log(\text{Age}) = 0.05$, and a metallicity of $Z/Z_\odot = 0.02$ as in Forrest et al. (2020a,b). For the assumed SFH, we adopt a double-exponential SFH as used in Forrest et al. (2020a,b).

Remarkably, regardless of the photometric dataset used, SFH assumed, underlying SED code, or range of free parameters, we find *all* best-fit SEDs result in a massive galaxy with a stellar mass of $\log(M_\star/M_\odot) \sim 11$. Across the various fits, UMG-28740 has a median mass of $\log(M_\star/M_\odot) = 10.98$ with a 1σ standard deviation of 0.09 (see Table 2 for measurements from each SED fit). Hereinafter, we conservatively use this stellar mass and error as our best estimate for UMG-28740. This SED fitting analysis also highlights a discrepancy between SFR and dust extinction – resulting in the two possible scenarios, star-forming or quenched (see §4.1 for a more detailed discussion).

3.2. An Overdense Region around UMG 28740

UMG-28740 is embedded within a significant overdensity at $z \sim 5$, as traced by the surface density of galaxies at $4.5 < z_{phot} < 5.5$ in the CANDELS photometric catalog. As shown in Figure 3, UMG-28740 resides near the center of the overdense region and is the most massive member. However, we caution that the observed overdensity is located near the edge of the CANDELS survey area within the EGS, with UMG-28740 only $\sim 16''$ from the edge of the *HST*/WFC3 imaging footprint, such that the full extent of the structure may be underestimated. Naidu et al. (2022) first identified this particular overdense region, finding that a ~ 0.8 arcmin^2 area centered on a lower-mass photometric neighbor of UMG-28740 contained 4× the average surface density of sources at $4.5 < z_{phot} < 5.5$. However, this lower-mass neighbor ($M_\star \sim 10^{9.6}$ M$_\odot$, spectroscopically confirmed by Arrabal Haro et al. 2023b), is located $\gtrsim 20''$ to the south ($\gtrsim 0.8$ cMpc at $z = 5$) of UMG-28740 and outside of the apparent center of the overdense region as traced by the CANDELS photometric catalog (see the highlighted red cross in Fig. 3).

To investigate the extent of the overdense region around UMG-28740, we search for other overdensities across the entire CANDELS footprint within the EGS field by comparing the galaxy surface densities in redshift slices of $\Delta z = 1$ to the average surface density at each corresponding epoch. We use the CANDELS catalog to identify sources at $2.5 < z_{phot} < 6.5$, as this catalog covers a larger footprint within the EGS (versus CEERS). We limit this analysis to sources with $\log(M_\star/M_\odot) > 9$, so as to define a tracer population that is unbiased (complete) over the full redshift range probed. Across the entire field, we compute the galaxy surface density as a function of position on the sky within an aperture of $45'' \times 45''$ and a depth of $\Delta z = 1$. Stepping through redshift from $z = 3$ to $z = 6$ with a step size of $\Delta z = 0.1$, we identify regions that are overdense compared to the average surface density at the corresponding redshift. We find that the region hosting UMG-28740 is one of the most extreme overdense regions within the EGS at $3 < z < 6$, with a surface density
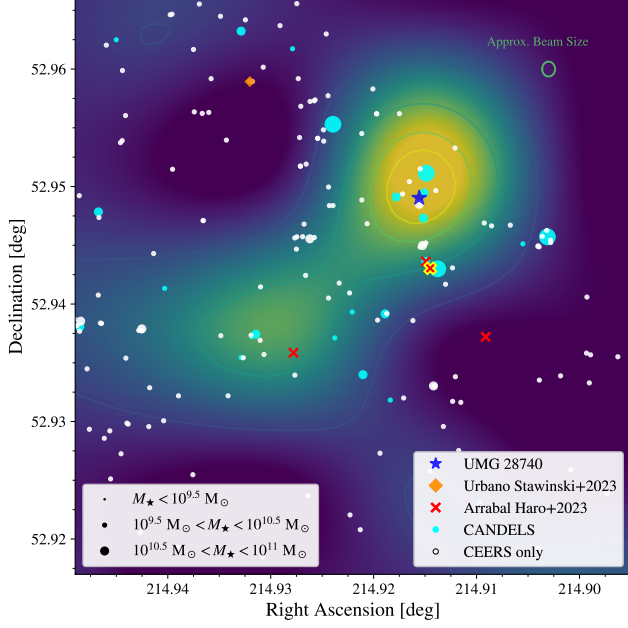
FIG. 3.— Overdensity hosting UMG-28740 (blue star) at $z \sim 5$. The underlying 2D histogram and contours show the galaxy surface density for objects in the CANDELS catalog at $4.5 < z_{\rm phot} < 5.5$ and $\log(M_\star/M_\odot) > 9$. The beam size (with a diameter of $4.5''$) used to convolve the density map is shown in the upper right corner. Cyan circles denote photometric sources found in the CANDELS (Stefanon et al. 2017) and CEERS (Bagley et al. 2023) catalogs, where white circles are low-mass galaxies only found in the deeper CEERS catalog. The size of the circle indicates the estimated stellar mass of the object. Red crosses and the orange diamond are spectroscopically-confirmed sources from Arrabal Haro et al. (2023a) and Urbano Stawinski et al. (2024), respectively. The highlighted red cross indicates the location of the lower-mass member from Naidu et al. (2022).

that is $\sim 10\times$ higher than the average surface density of the field at $z = 4.9$.

At $z \sim 5$, the effective radii of protoclusters are estimated to extend up to $R_e = 5 - 10$ cMpc (Chiang et al. 2013). UMG-28740 is positioned nearby the apparent center of the overdense region, such that we can estimate $R_{\rm proj}$ from UMG-28740 to trace the effective radius of the protocluster. However, we caution this region is also near the edge of the EGS field, limiting observed galaxies past $R_{\rm proj} \sim 0.6$ cMpc to the north-west and potentially skewing the true center of the overdensity. Nevertheless, within $R_{\rm proj} = 3.44$ cMpc from UMG-28740, there are 26 photometric protocluster members at $4.5 < z < 5.5$ and with $M_\star > 10^9$ M$_\odot$ in the CANDELS photometric catalog along with 160 members identified in the CEERS catalog, pushing down to lower stellar masses ($M_\star > 10^8$ M$_\odot$). Additionally, out of all the photometric members there are 4 massive neighbors with $10.5 < \log(M_\star/M_\odot) < 11$ within just $29.5''$, or ~ 1.13 cMpc, of UMG-28740. The closest of these massive members is only separated from UMG-28740 by 0.29 cMpc. This makes the protocluster surrounding UMG-28740 the most compact overdensity of massive $\log(M_\star/M_\odot) > 10.5$ galaxies within the entire EGS at $z \sim 5$ (according to the CANDELS catalog), with only two other compact regions each containing two similarly massive galaxies at a similar spatial scale ($R_{\rm proj} < 3$ cMpc). Moreover, there are *no* other instances of > 3 massive galaxies within $R_{\rm proj} < 3$ cMpc at this redshift in the CANDELS catalog.

This protocluster also hosts 5 spectroscopically-confirmed galaxies from Keck/DEIMOS (Urbano Stawinski et al. 2024)

TABLE 2
Stellar Mass and SFR from Alternative SED Fits

SFH	Code	Mass $\log(M_\star/M_\odot)$	SFR M$_\odot$/yr
CANDELS (Stefanon et al. 2017)			
Double-power law[a]	BAGPIPES	$11.08_{0.1}^{0.08}$	$285.0_{79.5}^{125.5}$
Double-power law+AGN	BAGPIPES	$10.97_{0.04}^{0.04}$	$8.6_{2.4}^{3.9}$
Double-power law+burst	BAGPIPES	$10.98_{0.09}^{0.08}$	$419.6_{162.2}^{156.7}$
Double-power law at $Z_\odot$	BAGPIPES	$11.18_{0.09}^{0.07}$	$299.9_{60.1}^{99.5}$
Delayed-τ	BAGPIPES	$10.92_{0.13}^{0.11}$	$312.1_{106.2}^{159.1}$
Double Exponential	FAST++	$10.95_{0.11}^{0.00}$	$24.5_{3.3}^{16.6}$
CEERS (Bagley et al. 2023)			
Double-power law[a]	BAGPIPES	$10.98_{0.03}^{0.04}$	$9.5_{2.7}^{4.8}$
Double-power law+AGN	BAGPIPES	$10.96_{0.04}^{0.04}$	$0.0_{0.0}^{0.0}$
Double-power law+burst	BAGPIPES	$11.17_{0.04}^{0.03}$	$18.1_{4.7}^{6.2}$
Double-power law at $Z_\odot$	BAGPIPES	$11.17_{0.03}^{0.03}$	$21.0_{19.0}^{9.9}$
Delayed-τ	BAGPIPES	$11.05_{0.03}^{0.02}$	$32.2_{5.7}^{10.8}$

[a] SED fit is shown in Fig. 2.

and *JWST*/NIRSpec (Arrabal Haro et al. 2023a) spectroscopy within $R_{\rm proj} = 3.44$ cMpc (see Fig. 3). The measured mass of these spectroscopic members range from $\log(M_\star/M_\odot) = 9.18 - 9.95$ and span 0.75 cMpc to 2.10 cMpc from UMG-28740. In summary, all members within $R_{\rm proj} = 4$ cMpc, both spectroscopically confirmed and all photometric candidates, are estimated to be less massive than UMG-28740.

4. DISCUSSION

4.1. *Investigation into Competing Star Formation Histories*

As mentioned in §3.1, the two sets of photometry yield two different SFH scenarios, one with a highly star-forming and dusty SED versus one with low star formation and little dust extinction. The high-quality *JWST*/NIRCam photometry favors a nearly quenched, SED. In contrast, the photometry from CANDELS favors a star-forming SED, with the exception of a quenched solution when assuming a double-exponential SFH with FAST++ (as described in §3.1). We show a variety of these SFHs, highlighting the best fit SEDs from the final BAGPIPES run, in Figure 4.

Looking at the SED fits alone, the $\pm 1\sigma$ spread of the orange, quenched SED is consistent with both sets of photometry within the errors. However, there is a clear offset between the *JWST*/NIRCam photometry and the blue, star-forming SED, with the largest discrepancy at F277W and F410M. To test the consistency between the NIRCam photometry and the star-forming SED, we predict the flux that we would expect from a mock F277W, F356W, F410M, and F444W observation of the star-forming SED fit, using the 'predict' function within the BAGPIPES code (see the open blue crosses in Fig. 2). For F277W, the expected flux would be elevated from the continuum due to the emission lines nearby $2.77\mu m$; however, we find this predicted flux is insufficient to reproduce the observed F277W flux even within $\pm 1\sigma$. For F356W and F410M, the predicted flux is elevated to a greater extent, due to contributions from strong emission lines such as Hα at $\sim 3.9\mu m$. However, this added emission over-predicts the flux measured by the NIRCam photometry (also seen, to a lesser extent, in
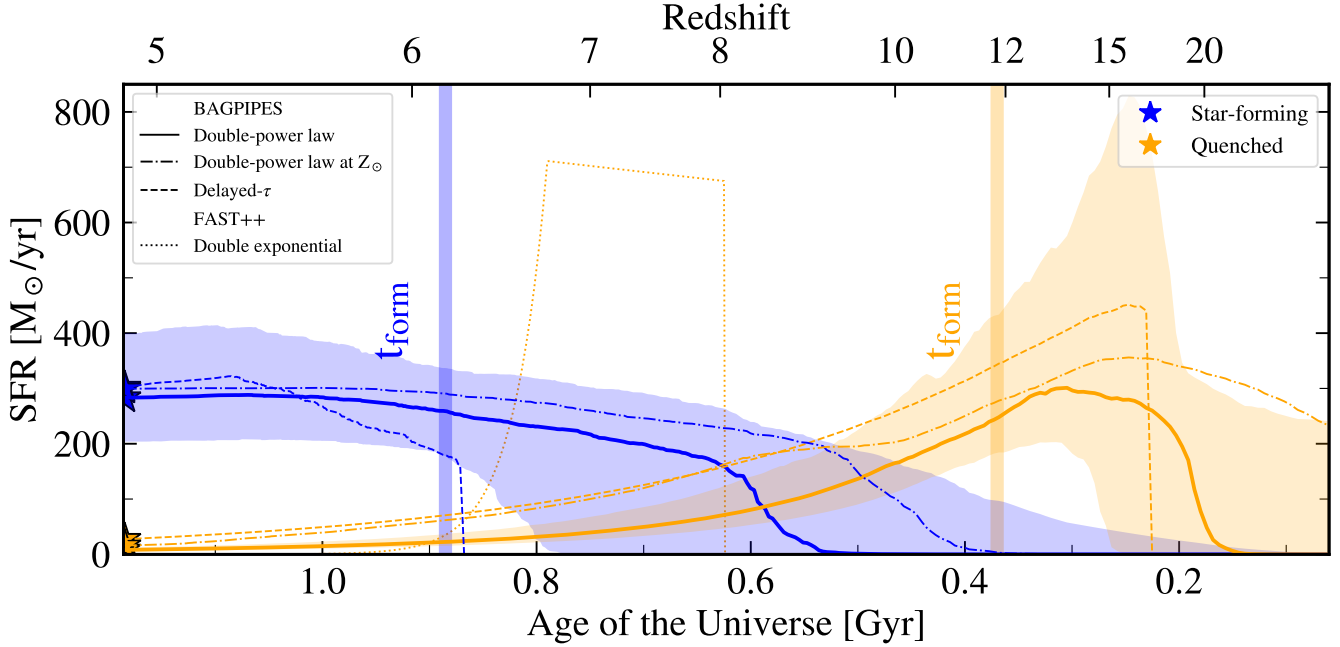
Fig. 4.— Star formation histories for the two competing scenarios, star-forming (blue) and quenched (orange), based on the best-fit SEDs from BAGPIPES and FAST++ (see Table 2). The solid lines, as well as the shaded region, show the best-fit and $\pm 1\sigma$ double-power law SFH from BAGPIPES (shown in Fig. 2). The formation time ($t_{\rm form}$) corresponds to the epoch at which 50% of the stellar mass is formed for the double-power law models. The higher-quality *JWST*/NIRCam photometry favors the quenched scenario and suggests that UMG-28740 formed much of its stellar mass as early as $z \gtrsim 10$.

the F444W predicted flux). Taken together, this suggests that the quenched scenario is more consistent with the observed photometry from both catalogs, and thus more likely to be the true SFH of UMG-28740.

One argument against a quenched SFH is the detection of Lyα emission. However, this may be explained by either AGN contribution or remnant star formation consistent with a post-starburst SED. Assuming no AGN contamination, we again use the 'predict' function in BAGPIPES to estimate the equivalent width (EW) of Lyα in the various SED fits. For the nearly quenched scenario, the SFR from all models without an AGN component ranges from 9.5 M$_\odot$ yr^{-1} to 32.2 M$_\odot$ yr^{-1}. Measuring the EW of Lyα from the model SEDs (using the $\pm 1\sigma$ spread in the quenched models) yields an EW$_{\rm Ly\alpha}$ = 16.5 − 42.7Å. We then estimate the EW of the observed Lyα line from Keck/DEIMOS. We find the continuum level just redward of the line profile and calculate the EW using a custom python code. Because the continuum level is so low, we conservatively call this measurement an upper limit on the true EW. Performing this analysis yields an observed EW$_{\rm Ly\alpha}$ > 34.0Å, within the range of the predicted values for the post-starburst SED. Hence, we cannot rule out the nearly quenched scenario by detection of Lyα emission alone.

We perform the same analysis on the SEDs with AGN contribution. With AGN contribution we find the $\pm 1\sigma$ spread for the quenched SEDs yields EW$_{\rm Ly\alpha}$ = 29.9 − 31.7Å, which is below the estimated observed Lyα EW. This would suggest that AGN contribution alone may not explain the presence of Lyα emission seen in the Keck/DEIMOS spectroscopy, and that likely there is some remnant star formation (even with the presence of AGN contamination).

The best-fit SEDs for UMG-28740 yield two different SFH scenarios, a highly star-forming galaxy or a nearly quiescent one. However, due to the flux required by the *JWST*/NIRCam

photometry in the mid-IR (F277W, F356W, F410M, and F444W) and the consistency in the EW of the observed and predicted Lyα emission line, we argue that the quenched SED is likely the true SFH of this object.

4.2. *Comparison to Simulations*

The number density of UMGs at $z \sim 5$ is extremely low, especially for more quiescent systems (Stefanon et al. 2015; Davidzon et al. 2017; Marsan et al. 2022; Weaver et al. 2023). In addition, due to various observational challenges associated with observing these systems, there are only a handful of spectroscopically-confirmed UMGs at this epoch in the literature (e.g. Antwi-Danso et al. 2023; Xiao et al. 2023; Carnall et al. 2023). To compare the SFR of UMG-28740 to a large, unbiased sample of galaxies, we plot SFR versus stellar mass for UMG-28740 with simulated galaxies. Many simulations struggle to produce massive systems at high redshift, and most fail to quench these objects at early epochs. However, the Illustris TNG-300 simulation (Nelson et al. 2019) has been able to form massive systems and subsequently suppress SFR to reproduce quiescent UMGs up to $z \sim 3.5$ (Forrest et al. 2020a; Schreiber et al. 2018; Glazebrook et al. 2017). Hence, we compare UMG-28740 to simulated galaxies in TNG-300 at $z = 5$ (see Fig. 5).

While TNG-300 reproduces massive quiescent systems at $z \sim 3.5$, as well as massive star-forming galaxies at earlier epochs (Forrest et al. 2020a), TNG-300 fails to create massive and quiescent galaxies like UMG-28740 (assuming a quenched scenario) and one other spectroscopically-confirmed quenched system in the literature (Carnall et al. 2023) at $z \sim 5$. The measured SFR of UMG-28740 for the quenched scenario is ~ 2 dex below that of any other simulated galaxy at $\log(M_\star/M_\odot) \sim 11$. On the other hand, the TNG-300 simulation does reproduce massive, star-forming galaxies at this epoch, including those from Xiao et al. (2023) and the star-forming scenario of UMG-
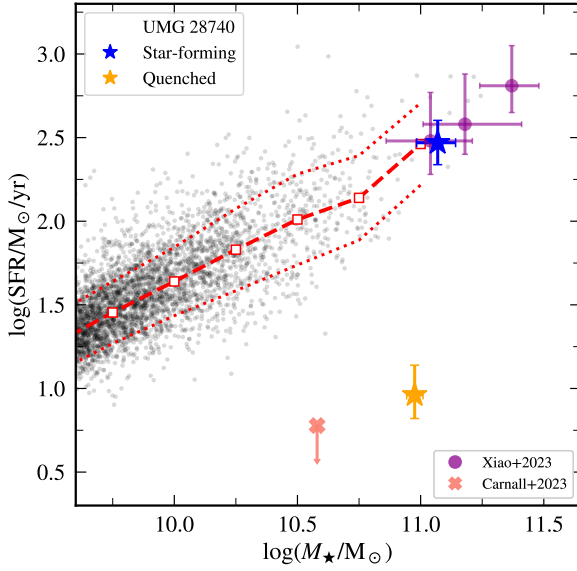
FIG. 5.— SFR versus stellar mass of UMG-28740 for the two scenarios, star-forming (blue star) and quenched (orange star). The black circles show galaxies from the Illustris TNG-300 simulation at $z = 5$. The red dashed line and white squares trace the median of the galaxies in the TNG sample, while the red dotted lines show the $\pm 1\sigma$ spread. We also include other spectroscopically-confirmed massive galaxies at this epoch from the literature as purple circles (Xiao et al. 2023) and a peach cross (Carnall et al. 2023).

28740. The lack of massive quenched objects is likely a result of one of two possibilities: the TNG-300 simulation fails to catch the cessation of star formation at this epoch or that the size of TNG-300 is too small ($V = 302.6^3$ Mpc^3) to capture a system as rare as UMG-28740 and its protocluster environment.

Recently, Xie et al. (2024) used the GAEA semi-analytic model (De Lucia et al. 2024), applied to a larger box size than that of TNG-300 ($V = 685^3$ Mpc^3), to study the formation of massive quiescent galaxies at early cosmic times. In summary, Xie et al. (2024) find a larger relative number of quenched massive galaxies at $z \sim 4.5$, with a quenched fraction for systems with $M_\star = (0.8 - 1.2) \times 10^{11}$ M$_\odot$ of $f_q \sim 0.06$. Xie et al. (2024) suggest that the primary quenching mechanism for massive galaxies at high redshift is accretion disk feedback via quasar winds. Yet even within the GAEA simulation UMG-28740 is exceptionally rare; galaxies as quiescent as the best-fit quenched model, with a specific SFR of $\sim 10^{-10}$ yr^{-1}, have a number density of only $\sim 2 \times 10^{-7}$ per cMpc^3 at $z \sim 5$ in GAEA (De Lucia et al. 2024).

4.3. *Mass Assembly History of UMG-28740*

To investigate the potential evolution of UMG-28740, in Figure 6 we plot the mass assembly history corresponding to the best-fit star-forming and quiescent models from BAGPIPES (see Fig. 4). We compare the mass growth of UMG-28740 to that of spectroscopically-confirmed UMGs at $z \sim 3.5$ from the Massive Ancient Galaxies At $z > 3$ NEar-infrared (MAGAZ3NE) survey (Forrest et al. 2020a,b, 2022), a Keck/MOSFIRE effort that has successfully spectroscopically confirmed a large sample of star-forming and quenched UMGs at $z \sim 3.5$. We also include a sample of massive dusty star-forming galaxies (DSFGs) at $z > 5$ from the literature (Riech-

ers et al. 2020; Williams et al. 2019; Jin et al. 2019; Zavala et al. 2018; Pavesi et al. 2018; Riechers et al. 2017; Strandet et al. 2017; Ma et al. 2015; Cooray et al. 2014; Riechers et al. 2013; Walter et al. 2012), including the dusty star-forming UMGs spectroscopically confirmed by Xiao et al. (2023). Finally, we also include the massive, spectroscopically-confirmed quiescent galaxy from Carnall et al. (2023) and the photometric massive galaxy candidates from Labbé et al. (2023). Below we discuss the possible connections between UMG-28740 and these various populations.

For the mass assembly history predicted by the best-fit star-forming models, UMG-28740 is consistent with being the progenitor of the existing UMG population at $z \sim 3.5$, such that the ongoing star formation in the system will continue to grow its stellar mass at $3 \lesssim z \lesssim 5$, likely becoming similar to one of the more massive UMGs detected by the MAGAZ3NE survey. Similarly, the DSFG population at $z \sim 5$, including the galaxies identified by Xiao et al. (2023), are also likely to evolve into members of the existing UMG population at $z \sim 3.5$ (Forrest et al. 2020b). Looking towards higher z for the best-fit star-forming models, the assembly history of UMG-28740 is consistent with the massive galaxy candidates from Labbé et al. (2023) as potential progenitors, with UMG-28740 forming much of its stellar mass at $z \lesssim 8$.

On the other hand, assuming the more-likely quenched SFH, UMG-28740 will evolve into a lower-mass UMG at $z \sim 3.5$ ($M_\star \sim 10^{11}$ M$_\odot$). Interestingly, however, in this scenario UMG-28740 would not be included in the sample of known UMGs at $z \sim 3.5$. Due to the difficulty in detecting absorption lines in faint systems from the ground, MAGAZ3NE observations were limited to an AB magnitude of $K_s < 21.7$. In contrast, if we passively evolve the quenched model SED for UMG-28740 at $z = 4.8947$ to $z = 3.5$, we find that UMG-28740 would have an AB magnitude of $K_s = 22.7$, fainter than the selection limit for the MAGAZ3NE survey and indicating that existing samples of UMGs at intermediate redshift may be biased against the oldest systems (see Forrest et al. 2020b). Instead, UMG-28740 would more likely resemble much fainter UMGs at $z \sim 3$, such as those that have been targeted with *JWST*/NIRSpec (Nanayakkara et al. 2024; Glazebrook et al. 2024).

Towards high-z, the evolutionary history of UMG-28740 drastically changes assuming a quenched model. At $z \sim 5$, UMG-28740 is already an extreme system, more massive than the only other spectroscopically-confirmed quiescent system at this epoch (Carnall et al. 2023). Moreover, in contrast to the massive quiescent galaxy from Carnall et al. (2023), which formed its mass at $z \sim 7$, we find UMG-28740 to already be quenching by $z \sim 8$, with the bulk of its stellar mass formed at much earlier cosmic time ($z > 10$). Based on the quenched SED fits, the mass assembly of UMG-28740 is inconsistent with the DSFG population at $z > 5$ and the massive galaxy candidates from Labbé et al. (2023), instead forming a more extreme amount of mass at very high redshift.

The formation of such massive galaxies at high redshift is a highly active area of study thanks to a wealth of new observations from *JWST*. For example, early *JWST* imaging campaigns discovered a surplus of massive galaxy candidates at $z = 8 - 14$ that stand in tension with predictions from ΛCDM (Casey et al. 2023; Labbé et al. 2023; Boylan-Kolchin 2023). These results have sparked a myriad of questions and scrutiny in our current understanding of the physical processes driving galaxy evolution, including those that underpin SED fitting codes. The extreme build-up of mass required to assemble
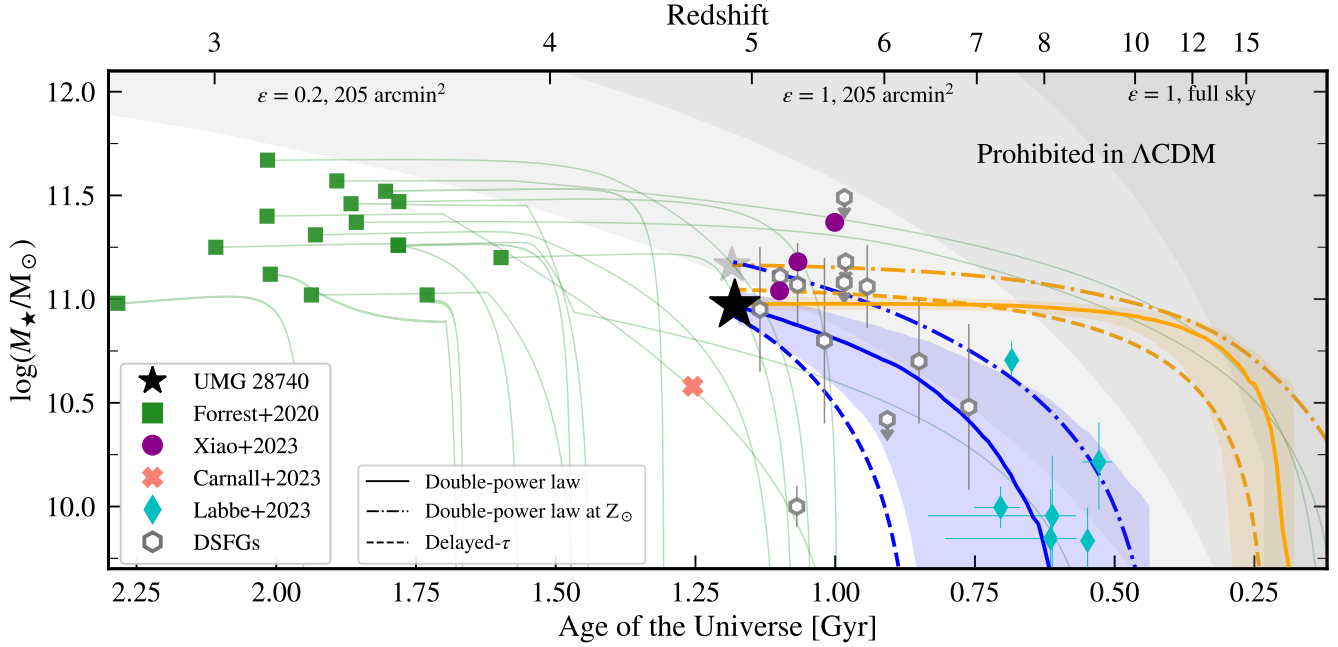
FIG. 6.— Mass assembly history of UMG-28740 for the best-fit star-forming models (blue lines) and quiescent models (orange lines). We include the double-power law fits (solid line), the fixed $Z = Z_\odot$ double-power law fits (dashed dotted lines), and the delayed-τ fits (dotted lines). The $\pm 1\sigma$ uncertainties for the double-power law fits are shown as the shaded blue and orange regions. The green tracks and squares show the assembly histories for spectroscopically-confirmed UMGs at $z \sim 3$ from Forrest et al. (2020b). Spectroscopically-confirmed massive galaxies at $z \sim 5$ from Xiao et al. (2023) and (Carnall et al. 2023) are shown as purple circles and a peach cross, respectively. Finally, we include a sample of $z > 5$ DSFGs (grey open hexagons) from the literature and a sample of photometric massive galaxy candidates from Labbé et al. (2023) (cyan diamonds). The grey shaded regions show the stellar mass prohibited by ΛCDM cosmology, following $M_\star{}^{\rm max} = \epsilon\, f_b\, M_{\rm halo}{}^{\rm max}$ where ϵ is the star formation efficiency and f_b is the cosmic baryon fraction. We include three different thresholds, by assuming the area of the EGS at a 20% efficiency and a 100% efficiency as well as the area of the full sky and 100% efficiency.

massive galaxies suggests intense bursts of star formation that convert $> 20\%$ of the available baryons into stars (Steinhardt et al. 2016; Boylan-Kolchin 2023; Sun et al. 2023; Casey et al. 2023; Xiao et al. 2023; Antwi-Danso et al. 2023).

To investigate the star formation efficiency of UMG-28740, we plot the limiting mass as imposed by a ΛCDM cosmology (shown as the grey shaded regions in Fig. 6). To do this, we follow the methodology from Boylan-Kolchin (2023), first calculating the number density of halos of a given mass as a function of redshift using hmf[4], a python package that calculates the halo mass function at different redshifts (Murray 2014). We then find the maximum halo mass, given a survey volume, for which we would observe 1 such system. To convert to stellar mass, we follow $M_\star{}^{\rm max} = \epsilon\, f_b\, M_{\rm halo}{}^{\rm max}$, where f_b is the cosmic baryon fraction and ϵ is the efficiency of converting baryons into stars. We perform this calculation for the area of the CANDELS footprint within the EGS (205 arcmin^2, Stefanon et al. 2017) using a line-of-sight depth of $\Delta z = 2$ and an efficiency of 20% ($\epsilon = 0.2$) and 100% ($\epsilon = 1.0$). We also calculate the maximum stellar mass for observations across the full sky with an efficiency of 100%, which is the upper limit for what is allowed in a ΛCDM cosmology.

At $z \sim 5$, UMG-28740 has a stellar mass consistent with a relatively high star formation efficiency ($\sim 20\%$), comparable to that found in larger samples of massive galaxies at high redshift (e.g. Chworowsky et al. 2023). In contrast, recent analyses of massive star-forming galaxies at $z > 5$ find even more extreme star formation efficiencies ($\epsilon \sim 0.5$, Xiao et al. 2023; Casey et al. 2023). If UMG-28740 is quiescent at $z \sim 5$, then its evolution is also consistent with an elevated formation

efficiency at higher z. As shown in Figure 6, at $z \gtrsim 8$ where the quenched model for UMG-28740 is still star forming, the implied formation efficiency is on the order of (and potentially in excess of) unity, consistent with the expectations from models of feedback-free star formation (Dekel et al. 2023). Moreover, for the quenched model, UMG-28740 reaches significant tension with ΛCDM at even earlier times, exceeding $\epsilon = 1$ across the area of the full sky at $z \sim 15$. This suggests UMG-28740 formed its stars at nearly impossible rates as currently predicted by theoretical models.

4.4. RUBIES-EGS-QC-1

While we finalized this manuscript, de Graaff et al. (2024) presented a JWST/NIRSpec PRISM and G395M spectrum of UMG-28740 (identified as RUBIES-EGS-QC-1 in de Graaff et al. 2024). The spectroscopic observations were collected in March 2024, with coverage of the Balmer break and the Hα emission line. This effort was part of the RUBIES survey (GO-4233; PIs A. de Graaff and G. Brammer), which uses JWST/NIRSpec to observe galaxies in the EGS and UDS fields. In this section, we discuss the results of this independent work and compare those to our work.

The physical properties of RUBIES-EGS-QC-1 were measured from SED fitting of the JWST/NIRSpec PRISM spectrum, as well as photometry from HST/WFC3 (F125W, F140W, and F160W), HST/ACS (F814W and F606W), and JWST/NIRCam (F115W, F150W, F200W, F277W, F356W, F444W, and F410M). The spectrum and photometry were fit simultaneously via Prospector (Leja et al. 2017), assuming a Chabrier IMF (Chabrier 2003), stellar population models from Flexible Stellar Population Synthesis (FSPS, Conroy & Gunn 2010; Conroy et al. 2009), the MILES spectral library

[4] https://hmf.readthedocs.io

(Sánchez-Blázquez et al. 2006), and MESA Isochrones and stellar tracks (MIST, Choi et al. 2016; Dotter 2016). With `Prospector`, de Graaff et al. (2024) explored four different star formation history models – a delayed-τ, rising, and fixed $Z = Z_\odot$ model as well as a SFH comprised of 14 bins of constant star formation. The resulting best-fit stellar mass is in agreement with our results, yielding $M_\star = 8.7^{+0.5}_{-0.4} \times 10^{10}$ $M_\odot$. With inclusion of mid-IR spectroscopy from $JWST$/NIRCam, de Graaff et al. (2024) pin down the SFR in the last 100 Myr as $SFR_{100} = 1.9^{+1.5}_{-1.0}$ $M_\odot$ yr^{-1}. This independent work uses a separate SED modeling code and includes a high-quality spectrum that probes key spectral features, yet the final results are in excellent agreement with our quenched model.

The complementary analysis from de Graaff et al. (2024), taken together with the conclusions of our SED fitting, highlights the importance of high-quality mid-IR photometry – currently only accessible via $JWST$/NIRCam – in understanding systems like UMG-28740. Only with such data can we accurately measure key physical properties of $z \gtrsim 4$ galaxies. This example (UMG-28740) demonstrates the importance of $JWST$ as we continue to search and study the rarest and most massive systems in the Universe.

5. CONCLUSIONS

In this work, we present spectroscopic confirmation of an ultra-massive galaxy (UMG, ID 28740) with $\log(M_\star/M_\odot) = 10.98 \pm 0.09$ at $z_{spec} = 4.8947$ based on deep spectroscopy with Keck/DEIMOS. UMG-28740 is one of the most massive spectroscopically-confirmed galaxies at $z \sim 5$ and lies within one of the most extreme overdensities in the EGS. Here, we summarize the main results of our analysis:

- Using the spectroscopic redshift, we run a large suite of SED modeling (assuming various SFHs and using two SED fitting codes, `BAGPIPES` and `FAST++`) on two sets of photometric data from CANDELS (Stefanon et al. 2017) and CEERS (Bagley et al. 2023). Regardless of the SED code, set of free parameters, or SFH assumed, the stellar mass of UMG-28740 is tightly constrained, with a median mass of $\log(M_\star/M_\odot) = 10.98$ and a standard deviation of ± 0.09 between all runs.

- We find a discrepancy between the measured SFR and photometric dataset assumed, with multiple SED fits to the CANDELS photometry yielding a highly star-forming object. However, when fitting to the $JWST$/NIRCam photometry from CEERS, UMG-28740 is nearly quiescent, with SFR < 32.2 $M_\odot$ yr^{-1}. Futhermore, while the quenched SED is consistent with both sets of photometry, the predicted flux from the best-fit star-forming SED is under-predicts the measured flux at F277W and over-predicts the measured flux at F356W, F410M, and F444W; suggesting a quenched scenario is more likely. Finally, we show the presence of Lyα does not rule out a post-starburst, nearly quenched scenario.

- We find UMG-28740 to be the most massive member of a protocluster environment at $z \sim 5$, with the surface density of galaxies in the region around UMG-28740 roughly 10× higher than the average coeval field surface density. Within $R_{proj} = 3.44$ cMpc of UMG-28740, we find 26 photometric members with $M_\star > 10^9$ $M_\odot$ and 160 photometric members with $M_\star > 10^8$ $M_\odot$ at $4.5 < z < 5.5$, using the CANDELS and CEERS photometric catalogs, respectively. Finally, we find four additional massive galaxies ($M_\star > 10^{10.5}$ $M_\odot$) within $0.29 - 1.13$ cMpc of UMG-28740 in the CANDELS photometric catalog.

- Comparing the SFR of UMG-28740 to the Illustris TNG-300 simulation box at $z = 5$ shows that, if quenched, UMG-28740 is extremely rare – with a SFR ~ 2 dex lower than any simulated galaxy at $\log(M_\star/M_\odot) \gtrsim 11$.

- We find UMG-28740 has a high star formation efficiency ($\sim 20\%$) at $z \sim 5$. Assuming a quenched model, this efficiency exceeds $\epsilon = 1$ for the area of the full sky, suggesting UMG-28740 would need to form its stars at faster rates than predicted by theoretical models.

REFERENCES

Antwi-Danso J., et al., 2023, arXiv e-prints, p. arXiv:2307.09590
Arrabal Haro P., et al., 2023a, Nature, 622, 707
Arrabal Haro P., et al., 2023b, ApJ, 951, L22
Bagley M. B., et al., 2023, ApJ, 946, L12
Baugh C. M., 2006, Reports on Progress in Physics, 69, 3101

Beichman C. A., Rieke M., Eisenstein D., Greene T. P., Krist J., McCarthy D., Meyer M., Stansberry J., 2012, in Clampin M. C., Fazio G. G., MacEwen H. A., Oschmann Jacobus M. J., eds, Society of Photo-Optical Instrumentation Engineers (SPIE) Conference Series Vol. 8442, Space Telescopes and Instrumentation 2012: Optical, Infrared, and Millimeter Wave. p. 84422N, doi:10.1117/12.925447
Boylan-Kolchin M., 2023, Nature Astronomy, 7, 731

Bruzual G., Charlot S., 2003, MNRAS, 344, 1000
Calzetti D., Armus L., Bohlin R. C., Kinney A. L., Koornneef J.,
    Storchi-Bergmann T., 2000, ApJ, 533, 682
Carnall A. C., McLure R. J., Dunlop J. S., Davé R., 2018, MNRAS, 480,
    4379
Carnall A. C., et al., 2023, Nature, 619, 716
Casey C. M., et al., 2023, arXiv e-prints, p. arXiv:2308.10932
Chabrier G., 2003, Publications of the Astronomical Society of the Pacific,
    115, 763
Chiang Y.-K., Overzier R., Gebhardt K., 2013, ApJ, 779, 127
Choi J., Dotter A., Conroy C., Cantiello M., Paxton B., Johnson B. D., 2016,
    The Astrophysical Journal, 823, 102
Chworowsky K., et al., 2023, arXiv e-prints, p. arXiv:2311.14804
Conroy C., Gunn J. E., 2010, ApJ, 712, 833
Conroy C., Gunn J. E., White M., 2009, ApJ, 699, 486
Cooper M. C., Newman J. A., Davis M., Finkbeiner D. P., Gerke B. F., 2012,
    spec2d: DEEP2 DEIMOS Spectral Pipeline, Astrophysics Source Code
    Library, record ascl:1203.003 (ascl:1203.003)
Cooray A., et al., 2014, ApJ, 790, 40
Croton D. J., et al., 2006, MNRAS, 365, 11
Davidzon I., et al., 2017, A&A, 605, A70
De Lucia G., Fontanot F., Xie L., Hirschmann M., 2024, arXiv e-prints, p.
    arXiv:2401.06211
Dekel A., Sarkar K. C., Birnboim Y., Mandelker N., Li Z., 2023, MNRAS,
    523, 3201
Dotter A., 2016, The Astrophysical Journal Supplement Series, 222, 8
Faber S. M., et al., 2003, in Iye M., Moorwood A. F. M., eds, Society of
    Photo-Optical Instrumentation Engineers (SPIE) Conference Series Vol.
    4841, Instrument Design and Performance for Optical/Infrared
    Ground-based Telescopes. pp 1657–1669, doi:10.1117/12.460346
Finkelstein S. L., et al., 2023, ApJ, 946, L13
Forrest B., et al., 2020a, ApJ, 890, L1
Forrest B., et al., 2020b, ApJ, 903, 47
Forrest B., et al., 2022, ApJ, 938, 109
Glazebrook K., et al., 2017, Nature, 544, 71
Glazebrook K., et al., 2023, Nature, 628, 277
Grogin N. A., et al., 2011, ApJS, 197, 35
Jin S., et al., 2019, ApJ, 887, 144
Koekemoer A. M., et al., 2011, ApJS, 197, 36
Kriek M., van Dokkum P. G., Labbé I., Franx M., Illingworth G. D.,
    Marchesini D., Quadri R. F., 2009, ApJ, 700, 221
Kroupa P., Boily C. M., 2002, MNRAS, 336, 1188
Labbé I., et al., 2023, Nature, 616, 266
Leja J., Johnson B. D., Conroy C., van Dokkum P. G., Byler N., 2017, ApJ,
    837, 170
Ma J., et al., 2015, ApJ, 812, 88

Marsan Z. C., Marchesini D., Brammer G. B., Geier S., Kado-Fong E., Labbé
    I., Muzzin A., Stefanon M., 2017, The Astrophysical Journal, 842, 21
Marsan Z. C., et al., 2022, The Astrophysical Journal, 924, 25
Martin C. L., Dijkstra M., Henry A., Soto K. T., Danforth C. W., Wong J.,
    2015, ApJ, 803, 6
Murray S., 2014, HMF: Halo Mass Function calculator, Astrophysics Source
    Code Library, record ascl:1412.006
Muzzin A., et al., 2013a, ApJS, 206, 8
Muzzin A., et al., 2013b, ApJ, 777, 18
Naidu R. P., et al., 2022, arXiv e-prints, p. arXiv:2208.02794
Nanayakkara T., et al., 2024, Scientific Reports, 14, 3724
Nelson D., et al., 2018, MNRAS, 475, 624
Nelson D., et al., 2019, Computational Astrophysics and Cosmology, 6, 2
Newman J. A., et al., 2013, ApJS, 208, 5
Pavesi R., et al., 2018, ApJ, 861, 43
Planck Collaboration et al., 2016, A&A, 594, A13
Riechers D. A., et al., 2013, Nature, 496, 329
Riechers D. A., et al., 2017, ApJ, 850, 1
Riechers D. A., et al., 2020, ApJ, 895, 81
Rieke M. J., et al., 2003, in Mather J. C., ed., Society of Photo-Optical
    Instrumentation Engineers (SPIE) Conference Series Vol. 4850, IR Space
    Telescopes and Instruments. pp 478–485, doi:10.1117/12.489103
Sánchez-Blázquez P., et al., 2006, MNRAS, 371, 703
Schreiber C., et al., 2018, A&A, 618, A85
Stefanon M., et al., 2015, ApJ, 803, 11
Stefanon M., et al., 2017, ApJS, 229, 32
Steinhardt C. L., Capak P., Masters D., Speagle J. S., 2016, ApJ, 824, 21
Strandet M. L., et al., 2017, ApJ, 842, L15
Sun G., Faucher-Giguère C.-A., Hayward C. C., Shen X., Wetzel A.,
    Cochrane R. K., 2023, The Astrophysical Journal Letters, 955, L35
Urbano Stawinski S. M., et al., 2024, MNRAS, 528, 5624
Valentino F., et al., 2020, ApJ, 889, 93
Valentino F., et al., 2023, ApJ, 947, 20
Verhamme A., Schaerer D., Atek H., Tapken C., 2008, A&A, 491, 89
Walter F., et al., 2012, Nature, 486, 233
Weaver J. R., et al., 2023, A&A, 677, A184
Weibel A., et al., 2024, arXiv e-prints, p. arXiv:2403.08872
Weiner B. J., et al., 2006, ApJ, 653, 1027
Williams C. C., et al., 2019, ApJ, 884, 154
Wright A. H., et al., 2017, Monthly Notices of the Royal Astronomical
    Society, 470, 283
Xiao M., et al., 2023, arXiv e-prints, p. arXiv:2309.02492
Xie L., et al., 2024, arXiv e-prints, p. arXiv:2402.01314
Zavala J. A., et al., 2018, Nature Astronomy, 2, 56
de Graaff A., et al., 2024, arXiv e-prints, p. arXiv:2404.05683

This paper was built using the Open Journal of Astrophysics LATEX template. The OJA is a journal which provides fast and easy peer review for new papers in the `astro-ph` section of the arXiv, making the reviewing process simpler for authors and referees alike. Learn more at `http://astro.theoj.org`.